The Astrophysical Journal, 675: L49–L52, 2008 March 1

RELATIONSHIP BETWEEN EIT POSTERUPTION ARCADES, CORONAL MASS EJECTIONS, THE CORONAL NEUTRAL LINE, AND MAGNETIC CLOUDS

Vasyl Yurchyshyn
Big Bear Solar Observatory, 40386 North Shore Lane, Big Bear City, CA 92314
Received 2007 November 20; accepted 2008 January 18; published 2008 January 31

ABSTRACT

There is observational evidence that the elongation of an Earth-directed coronal mass ejection (CME) may indicate the orientation of the underlying erupting flux rope. In this study, we compare orientations of CMEs, magnetic clouds (MCs), EIT (EUV Imaging Telescope) posteruption arcades, and the coronal neutral line (CNL). We report on good correlations between (1) the directions of the axial field in the EIT arcades and the elongations of halo CMEs, and (2) the tilt of the CNL and MC axis orientations. We found that majority of the eruptions that had EIT arcades, CMEs, and MCs similarly oriented also had the CNL co-aligned with them. On the other hand, those events that showed no agreement between orientations of the EIT arcades, CMEs, and MCs had their MCs aligned with the CNL. We speculate that the axis of the ejecta may be rotated in such a way that it is locally aligns itself with the heliospheric current sheet.

Subject headings: solar-terrestrial relations — Sun: coronal mass ejections (CMEs) — Sun: flares — Sun: magnetic fields

Online material: color figures

1. INTRODUCTION

Earth-directed coronal mass ejections (CMEs), or full halos (Howard et al. 1982), are known to be associated with various, often hazardous, disturbances in the near-Earth environment. The key issue here is the presence in the ejecta of a strong southward component of the magnetic field, which is known to be associated with geomagnetic storms (Russell et al. 1974). Better knowledge of CMEs' magnetic structure is, therefore, crucial for our advance in the physical understanding and theoretical modeling of CME origins, as well as for space weather forecasts.

CMEs are thought to represent a flux rope (Burlaga et al. 1981; Chen & Garren 1993; Chen et al. 1997; Moran & Davila 2004; Krall & St. Cyr 2006; Krall 2007) and are highly structured three-dimensional features (Cremades & Bothmer 2004; Krall & St. Cyr 2006). The structured CMEs appear to be magnetically organized in the axial direction, which corresponds to the axis of a large-scale twisted flux rope. A recent study by Krall & St. Cyr (2006) showed that statistical parameters, measured for observed CMEs, such as eccentricity and the axial aspect ratio are in agreement with those obtained for a parameterized model flux rope.

White-light coronagraphs, such as the LASCO instrument on board the *SOHO* observatory, show that halo CMEs have various sizes and shapes. Many of them can be enveloped by an ellipse and can be fitted with a cone model (Zhao et al. 2002; Xie et al. 2004; Zhao 2005; Michalek et al. 2006).

Erupting-flux-rope modeling (Krall et al. 2006; Yurchyshyn et al. 2006, 2007) showed that model halo CMEs appear to be elongated in the direction of the underlying flux rope axial field. Therefore it is quite possible that the ellipse-shaped appearance of halo CMEs may be related to their magnetic structure.

Following this idea, we have measured the orientations of 25 ellipse-shaped halos and the associated magnetic clouds (MCs) and reported that for about 64% of events, the difference between the orientations of halo elongations and MCs does not exceed $\pm 45°$ (Yurchyshyn et al. 2007, hereafter Paper I). This finding was later confirmed by X. P. Zhao (2007, private communication).

This Letter is continuation of our research on the structure of erupting magnetic fields. Here we compare tilts of (1) EUV posteruption arcades (PEAs) usually associated with eruptions (Tripathi et al. 2004), (2) halo CMEs, (3) the heliospheric current sheet near the eruption site, and (4) the axial field in MCs at 1 AU, in order to further investigate CME evolution in interplanetary space.

2. METHOD AND MEASUREMENTS

2.1. *Orientations of Halo CMEs*

Our study is based on 25 events, selected from the Master Data Table compiled during the "Living with a Star" Coordinated Data Analysis Workshops (Zhang et al. 2007) and the list published in Qiu & Yurchyshyn (2005).

All orientation angles discussed in this study were determined in the geocentric solar ecliptic coordinate system (GSE), where the *y*-axis is in the ecliptic plane pointing toward dusk, the *x*-axis is directed from the Earth toward the Sun, and the *z*-axis is pointed northward. The CME orientation angle (tilt), $\alpha_{\rm CME}$, was determined in Paper I by fitting an ellipse to an irregularly shaped "halo" around the C3 occulting disk (Fig. 2 in Paper I) and measuring its tilt in the clockwise direction from the positive GSE *y*-axis to the ellipse semimajor axis (see inset in Figs. 1 and 3). Because we measured three to five LASCO frames for each event, the final CME tilt, listed in Table I of Paper I, was calculated as the mean of all angles, determined from individual frames. For the majority of CMEs the standard deviation of the measurements did not exceed 15° and is shown in the corresponding graphs.

2.2. *Direction of the Axial and Azimuthal Field in EUV Posteruption Arcades and CMEs*

In Paper I we did not take into account the possible direction of the axial field in a CME (i.e., the underlying erupting flux rope), so the CME orientations have 180° ambiguity in their direction. To remove the ambiguity we use the magnetic field

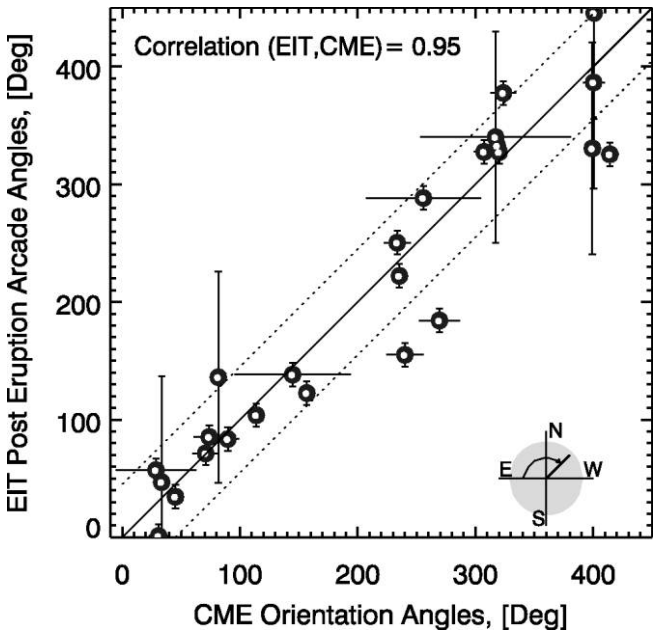

FIG. 1.—Correlation between the directions of the axial field in CMEs and EIT PEAs. Open error bars show standard deviation of the CME measurements, while closed bars are the absolute error of the PEA data. The inset in the lower right corner shows the coordinate system used to determine the orientation angles, which were measured from solar east toward the axes of an EIT arcade and a halo CME. Two dashed lines indicate $\pm 45°$ interval around the bisector. [*See the electronic edition of the Journal for a color version of this figure.*]

structure inferred from the associated PEA and require that the axial field of the PEA should make an acute angle with that of the CME, which can be achieved by adding 180° to the CME orientation angle. The "standard" flare model (e.g., see review by Forbes 2000) predicts that eruption of a flux rope is accompanied by magnetic reconnection and the formation of flare ribbons at the footpoints of the PEA (Tripathi et al. 2004; Qiu & Yurchyshyn 2005; Qiu et al. 2007), which indicate the general orientation of the erupting flux rope. The CME ambiguity resolution is based on the assumption that the direction of the axial field and twist in a flux rope CME corresponds to those of the EIT/Hα flare arcade associated with the eruption. In general, the direction of the axial field and twist (helicity sign) in a PEA can be determined from solar data (see details in Yurchyshyn et al. 2001). We estimated that in most cases PEA angles were measured with accuracy $\pm 10°$, although in six events the absolute error was estimated to be 90°.

In Figure 1 we show the correlation between the CME angles and PEA directions. For the overwhelming majority of events the difference between the angles is less that 45°. This indicates that, on average, the elongation of a halo CME is co-aligned with the EIT posteruption arcade and is additional evidence that the ellipse shape of a halo CME may indeed bear information on the geometry of the underlying flux rope. Because of this high correlation, for the comparisons with other parameters we only use CME orientations and we refer to them in the text below as PEA/CME orientations/angles.

2.3. *Orientation of the Coronal Neutral Line as Measured from Coronal Field Maps*

The background in Figure 2 is the Wilcox Solar Observatory coronal magnetic field map showing the polarity distribution (*light and dark gray*) during Carrington rotation (CR) 1968. The black solid line represents the major coronal neutral line

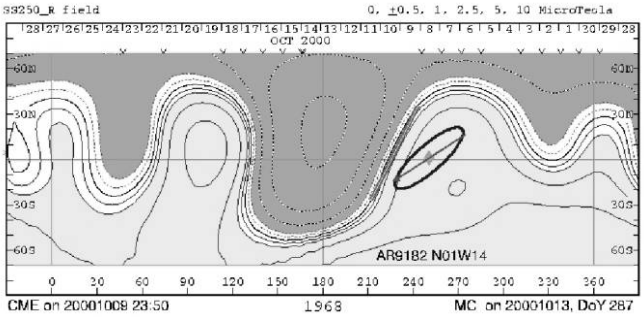

FIG. 2.—Wilcox Solar Observatory coronal field map calculated for the height of 2.5 $R_\odot$ for CR 1968. Dark grey contours represent negative fields, light gray contours, positive fields. Thick solid line is the CNL. The line segment shows the estimated orientation of the CNL near the site of eruption on 2000 October 13. The tilt of the CNL was measured in the clockwise direction from the east. The ellipse, centered at the location of the CME source (*diamond*), indicates the orientation of a halo CME. [*See the electronic edition of the Journal for a color version of this figure.*]

(CNL). This map was calculated from a synoptic photospheric field map with a potential field model (Hoeksema et al. 1983; Hoeksema 1984). The diamond in Figure 2 indicates the location of the CME source region relative to the CNL, i.e., on the day when it crossed the central meridian. The averaged tilt of the neutral line near the eruption site was measured (in clockwise direction) as the tilt of a thick line segment centered on the point closest to the eruption site.

In order to compare directional angles of CMEs and MCs with the tilt of the CNL, which has a 180° ambiguity, we needed to assign the direction to the CNL orientation. This was done the same way as we assigned the field direction in the CME: by requiring that the CNL directional angle makes an acute angle with the axial field of the corresponding MC. Our choice of MCs as a reference is justified as follows: (1) both MCs and the CNL are low-order, large-scale heliospheric structures, as opposed to the PEAs that represent high-order solar surface fields, and (2) it is not necessary that each PEA be formed under the streamer belt, and therefore the PEA orientation may not always be related to the CNL.

2.4. *Magnetic Cloud Parameters*

For each event, the MC orientation angle was obtained by averaging the orientations produced with different MC fitting routines (Paper I). The orientation (clock) angle is the direction angle of the projected MC flux rope axis onto the GSE y-z plane, measured in the clockwise direction from the positive y-axis. The current methodology and techniques used here allow us to determine the MC axis position with accuracy no better than 20°.

3. RESULTS

In Figure 3 we present a correlation between the CME orientations and MC axes. The green symbols indicate those 15 (out of 25) events that showed a good correspondence between the CME and MC directions (angle difference < 45°). The red symbols represent events where the angle difference exceeds 45°. Please, note that Figures 3, 4, and 5 use the same color coding. Figure 4 plots CME directions versus the CNL tilt. Similarly to Figure 3, the green symbols in this plot are also mainly clustered around the bisector (*solid line*). All "red" events in Figure 4, except two, are also located outside the $\pm 45°$ range centered on the bisector. Figures 3 and 4 imply

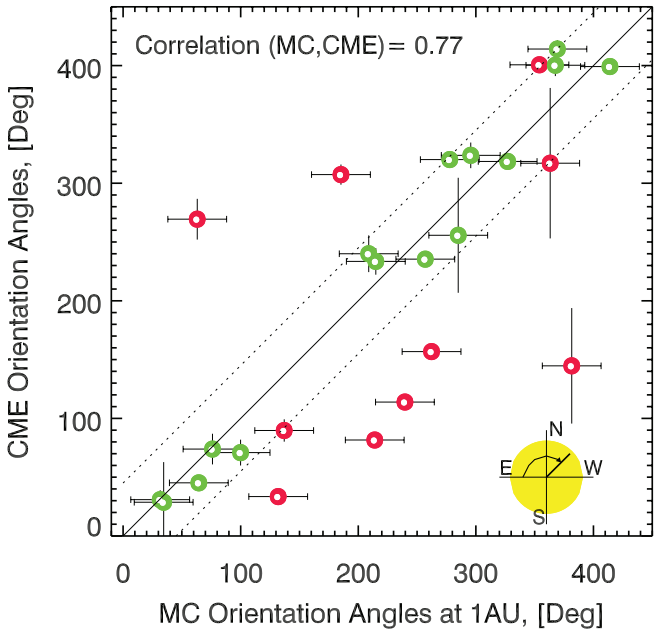

FIG. 3.—PEA/CME orientation angles plotted vs. the axial field directions in MCs. The green symbols indicate those events that showed a good correspondence (difference < 45°) between the two directional angles. Red symbols are the events that display no correspondence (difference > 45°). Open error bars show standard deviation of the CME measurements, while closed bars are the absolute error of the MC data. The inset in the lower right corner shows the coordinate system used to determine the orientation angles, which were measured from solar east toward the axes of a halo CME and an MC. Two dashed lines indicate ±45° interval around the bisector.

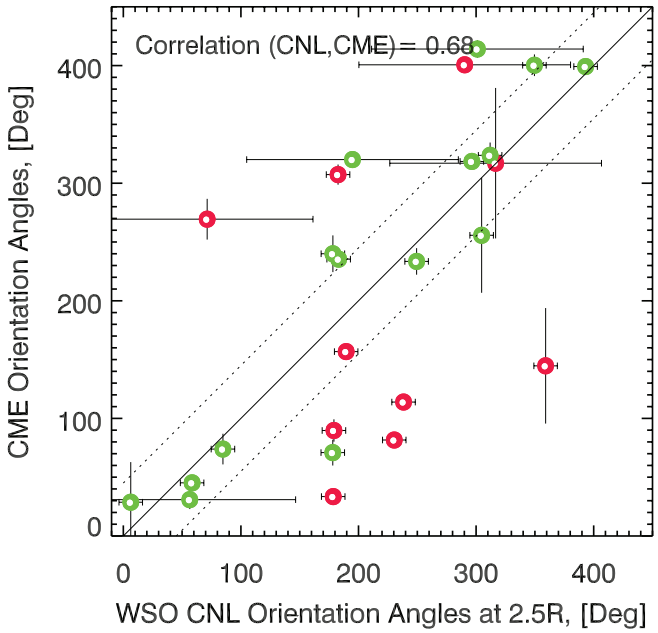

FIG. 4.—CME orientation angles plotted vs. the orientation of the CNL near the eruption site. The green/red symbols in this plot indicate the same events as in Fig. 3. Note that majority of green symbols are also located at or near the bisector. Open error bars show standard deviation of the CME measurements, while closed bars are the absolute error of the CNL data. Two dashed lines indicate ±45° interval around the bisector.

that those erupting flux ropes that where initially aligned with the CNL (streamer belt) at the early stage of eruption appear to remain so when they reach the Earth, and thus that their orientations match those of the MCs.

In Figure 5 we plot MC axis directions versus the tilt of the CNL near the eruption site. This graph displays a high correlation between the parameters with the data points tightly clustered around the bisector. The figure indicates that the MCs in our data set tend to be aligned along the CNL. Considering that the CNL is the base of the heliospheric current sheet, it ultimately means that the MCs were embedded in the current sheet.

4. CONCLUSIONS AND DISCUSSION

First, we would like to briefly summarize our findings: (1) there is a good correlation between the directions of the axial field in EIT posteruption arcades and the elongations of halo CMEs; (2) 80% of the events in the data set display the difference between CNL and MC orientations as less than 45°; (3) the majority of the eruptions that had PEA/CMEs and MCs similarly oriented (i.e., "green" events) also had the magnetic neutral line co-aligned with them; (4) those PEA/CME-MC pairs that showed no agreement between the PEA/CME and MC orientations ("red" events) had their MCs aligned with the magnetic neutral line.

As we mentioned earlier, observations and theoretical works indicate that the coronal ejecta may evolve substantially as it expands out into heliosphere and interacts with heliospheric and solar wind magnetic fields. Shape, structure, and magnetic field connectivity of the interplanetary ejecta may change due to interactions with ambient solar wind.

The data presented here show that CMEs may be significantly affected by the heliospheric magnetic fields: not only do they have a tendency to be deflected toward the heliomagnetic equator and channeled into the heliospheric current sheet (Crooker et al. 1993; Zhao & Hoeksema 1996; Mulligan et al. 1998; Kahler et al. 1999), but also the axis of the flux

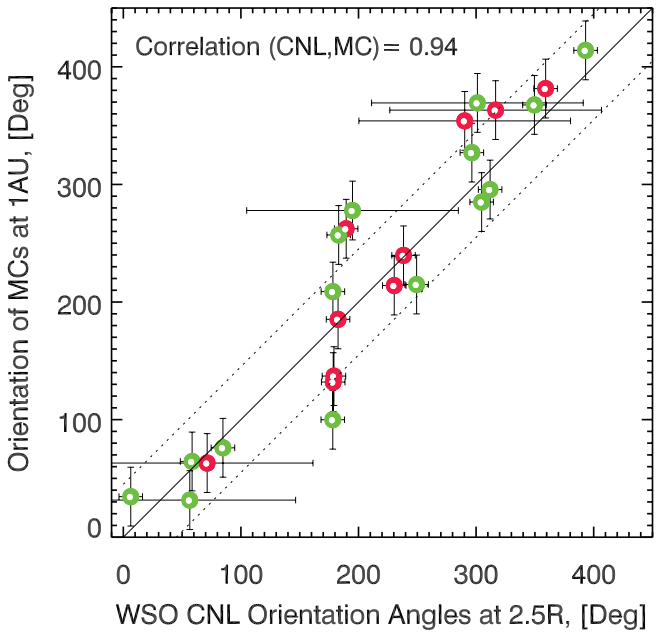

FIG. 5.—Directions of MC axial fields plotted vs. the orientation of the CNL. The green symbols indicate the same events as in Fig. 3. The majority of green and red symbols in this plot are located at or near the bisector. Two dashed lines indicate ±45° interval around the bisector.

rope appears to be locally aligned with the heliospheric current sheet. This inference, based on a detailed study of 25 events, is in agreement with the earlier reports that (1) MCs, oriented between $\pm 30°$, tend to be detected more frequently (Zhao & Hoeksema 1998), and that (2) during solar minimum (maximum), they dominate bipolar (unipolar) MCs (Mulligan et al. 1998). Note that bipolar (unipolar) MCs are nearly parallel (perpendicular) to the ecliptic.

To further explore these findings, we used coronal field models that show the shape and position of the neutral line at different heights above the solar surface. They were produced by the SAIC solar physics group (Riley et al. 2001). This model reasonably reproduces the global structure of the heliosphere in a qualitative fashion; however, quantitatively it might not be very accurate (Riley et al. 2002, 2003). The left panel in Figure 6 shows a coronal field map at 1.6 $R_\odot$ and the orientation of the halo CME (*ellipse*), while the right panel shows a coronal field map at 16.5 $R_\odot$ and the orientation of the corresponding MC (*arrow*). As follows from the figure, the CME elongation initially matched the local tilt of the neutral line. However, farther out from the Sun, the neutral line changes its orientation and, apparently, the interplanetary ejecta does the same, in such a way that the corresponding MC is well aligned with the neutral line. These model data seem to be consistent with the above indications that the heliospheric magnetic field may significantly influence coronal eruptions, although extended studies are needed to further explore this interaction.

One of the problems with this interpretation is that some CMEs originate from unipolar closed regions (Zhao & Webb 2003; Liu 2007) and are, thus, associated with the unipolar boundary layer. In this case the above explanation may not be valid since the heliospheric current sheet is not present.

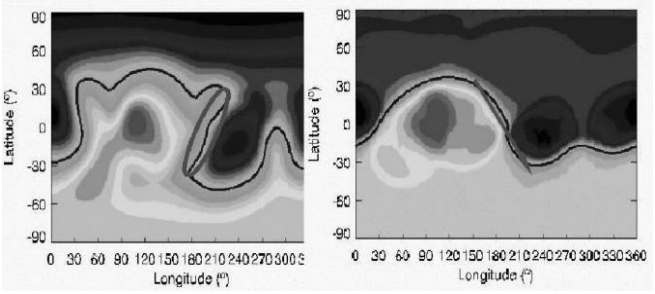

FIG. 6.—Coronal field maps calculated at 1.6 $R_\odot$ (*left*) and 16.5 $R_\odot$ (*right*) for CR 2006 by SAIC solar physics group. The thick black contour is the coronal magnetic neutral line. The oval represents a halo CME on 2003 August 14, aligned along the CNL at 1.6 $R_\odot$. The arrow in the right panel indicates the axis of the corresponding MC. [*See the electronic edition of the Journal for a color version of this figure.*]

The authors thank the reviewers of this manuscript for providing many critical comments and improvements that made this Letter clearer. The CME catalog is generated and maintained by the Center for Solar Physics and Space Weather, the Catholic University of America in cooperation with the Naval Research Laboratory, and NASA. We acknowledge the usage of the list of geomagnetic storms compiled during the "Living with a Star" Coordinated Data Analysis Workshops. We thank the *ACE* MAG and SWEPAM instrument teams and the *ACE* Science Center for providing the *ACE* data, and A. Szabo and F. Mariani of the *Wind* MFI team for data management and calibration. *SOHO* is a project of international cooperation between ESA and NASA. V. Y.'s work was supported under NSF grant 0536921 and NASA *ACE* NNG0-4GJ51G and LWS TR&T NNG0-5GN34G grants.

REFERENCES

Burlaga, L., Sittler, E., Mariani, F., & Schwenn, R. 1981, J. Geophys. Res., 86, 6673
Chen, J., & Garren, D. A. 1993, Geophys. Res. Lett., 20, 2319
Chen, J., et al. 1997, ApJ, 490, L191
Cremades, H., & Bothmer, V. 2004, A&A, 422, 307
Crooker, N. U., Siscoe, G. L., Shodhan, S., Webb, D. F., Gosling, J. T., & Smith, E. J. 1993, J. Geophys. Res., 98, 9371
Forbes, T. G. 2000, J. Geophys. Res., 105, 23153
Hoeksema, J. T. 1984, Ph.D. thesis, Stanford Univ.
Hoeksema, J. T., Wilcox, J. M., & Scherrer, P. H. 1983, J. Geophys. Res., 88, 9910
Howard, R. A., Michels, D. J., Sheeley, N. R., Jr., & Koomen, M. J. 1982, ApJ, 263, L101
Kahler, S. W., Crooker, N. U., & Gosling, J. T. 1999, J. Geophys. Res., 104, 9919
Krall, J. 2007, ApJ, 657, 559
Krall, J., & St. Cyr, O. C. 2006, ApJ, 652, 1740
Krall, J., Yurchyshyn, V. B., Slinker, S., Skoug, R. M., & Chen, J. 2006, ApJ, 642, 541
Liu, Y. 2007, Adv. Space Res., 39, 1767
Michalek, G., Gopalswamy, N., Lara, A., & Yashiro, S. 2006, Space Weather, 4(10), S10003
Moran, T. G., & Davila, J. M. 2004, Science, 305, 66
Mulligan, T., Russell, C. T., & Luhmann, J. G. 1998, Geophys. Res. Lett., 25, 2959
Qiu, J., Hu, Q., Howard, T. A., & Yurchyshyn, V. B. 2007, ApJ, 659, 758
Qiu, J., & Yurchyshyn, V. B. 2005, ApJ, 634, L121
Riley, P., Linker, J. A., & Mikic, Z. 2001, J. Geophys. Res., 106, 15889
———. 2002, J. Geophys. Res., 107, 1136
Riley, P., Mikic, Z., & Linker, J. A. 2003, Ann. Geophys., 21, 1347
Russell, C. T., McPherron, R. L., & Burton, R. K. 1974, J. Geophys. Res., 79, 1105
Tripathi, D., Bothmer, V., & Cremades, H. 2004, A&A, 422, 337
Xie, H., Ofman, L., & Lawrence, G. 2004, J. Geophys. Res., 109, A03109
Yurchyshyn, V., Hu, Q., Lepping, R. P., Lynch, B. J., & Krall, J. 2007, Adv. Space Res., 40, 1821 (Paper I)
Yurchyshyn, V., Liu, C., Abramenko, V., & Krall, J. 2006, Sol. Phys., 239, 317
Yurchyshyn, V. B., Wang, H., Goode, P. R., & Deng, Y. 2001, ApJ, 563, 381
Zhang, J., et al. 2007, J. Geophys. Res., 112, A10102
Zhao, X., & Hoeksema, J. T. 1996, J. Geophys. Res., 101, 4825
Zhao, X. P. 2005, in IAU Symp. 226, Solar and Steller Mass Ejections, ed. K. Dere, J. Wang, & Y. Yan (Cambridge: Cambridge Univ. Press), 42
Zhao, X. P., & Hoeksema, J. T. 1998, J. Geophys. Res., 103, 2077
Zhao, X. P., Plunkett, S. P., & Liu, W. 2002, J. Geophys. Res., 107(A8), 1223
Zhao, X. P., & Webb, D. F. 2003, J. Geophys. Res., 108(A6), 1234